Chin. Geogra. Sci. 2018 Vol. 28 No. 6 pp. 907–919
https://doi.org/10.1007/s11769-018-1002-2

Springer Science Press
www.springerlink.com/content/1002-0063

Detecting Global Vegetation Changes Using Mann-Kendal (MK) Trend Test for 1982–2015 Time Period

GUO Meng[1], LI Jing[2], HE Hongshi[1, 3], XU Jiawei[1], JIN Yinghua[1]

(1. *School of Geographical Sciences*, *Northeast Normal University*, *Changchun* 130024, *China*; 2. *Northeast Institute of Geography and Agroecology*, *Chinese Academy of Sciences*, *Changchun* 130102, *China*; 3. *School of Natural Resources*, *University of Missouri-Columbia*, *Columbia* 65211, *USA*)

Abstract: Vegetation is the main component of the terrestrial ecosystem and plays a key role in global climate change. Remotely sensed vegetation indices are widely used to detect vegetation trends at large scales. To understand the trends of vegetation cover, this research examined the spatial-temporal trends of global vegetation by employing the normalized difference vegetation index (NDVI) from the Advanced Very High Resolution Radiometer (AVHRR) Global Inventory Modeling and Mapping Studies (GIMMS) time series (1982–2015). Ten samples were selected to test the temporal trend of NDVI, and the results show that in arid and semi-arid regions, NDVI showed a deceasing trend, while it showed a growing trend in other regions. Mann-Kendal (MK) trend test results indicate that 83.37% of NDVI pixels exhibited positive trends and that only 16.63% showed negative trends ($P < 0.05$) during the period from 1982 to 2015. The increasing NDVI trends primarily occurred in tree-covered regions because of forest growth and re-growth and also because of vegetation succession after a forest disturbance. The increasing trend of the NDVI in cropland regions was primarily because of the increasing cropland area and the improvement in planting techniques. This research describes the spatial vegetation trends at a global scale over the past 30+ years, especially for different land cover types.

Keywords: vegetation trend; NDVI3g.v1; Mann-Kendall (MK) trend test; land cover types

Citation: GUO Meng, LI Jing, HE Hongshi, XU Jiawei, JIN Yinghua, 2018. Detecting Global Vegetation Changes Using Mann-Kendal (MK) Trend Test for 1982–2015 Time Period. *Chinese Geographical Science*, 28(6): 907–919. https://doi.org/10.1007/s11769-018-1002-2

1 Introduction

Over the past 50 years, the terrestrial ecosystem has been changed more rapidly and extensively than ever before, and vegetation represents the main component of this ecosystem. Vegetation change will directly affect the carbon cycle and climate change. There is compelling evidence that the deterioration of almost all terrestrial ecosystems is largely due to human activities and climate change (Stellmes et al., 2010; Yang et al., 2017). Barrow (2009) observed that vegetation degradation was usually expressed in terms of measurable physical or biological conditions or processes that can be used as surrogates for productivity loss. Vegetation degradation causes a reduction in the ability of land to support life, which affects wild species, domestic animals, agriculture, and human being. The reduction in vegetation cover that accompanies desertification has also led to soil erosion (El Hassan, 2004). Prince et al. (2009) agreed that there was significant vegetation degradation in certain areas and this degradation has powerful effects on the environment and human well-being. Vegeta-

Received date: 2018-03-09; accepted date: 2018-07-06
Foundation item: Under the auspices of National Natural Science Foundation of China (No. 41771179, 41871103, 41771138), the National Key Research and Development Project (No. 2016YFA0602301)
Corresponding author: LI Jing. E-mail: lijingsara@iga.ac.cn

tion trend is a good indicator of vegetation degradation and has been widely used on regional and global scales.

Vegetation change under global warming is currently an attractive research topic (Guo et al., 2013). Previous research has related land use changes and possible climate variability to the observed normalized difference vegetation index (NDVI) variation and found that seasonal NDVI variation could be used to distinguish land cover change based on greenness and that greenness has a weak relationship with precipitation (Neeti et al., 2012). Understanding the potential of vegetation cover to affect CO_2 accumulation in the atmosphere may be important for predicting climate change in the future (Zeng et al., 2013).

Vegetation changes could be inferred from a vegetation index, such as NDVI and enhanced vegetation index (EVI). NDVI, based on red and near-infrared reflectance (Tucker, 1979), is strongly correlated with vegetation productivity and has been the most widely used index in vegetation related studies over the past nearly 40 years. Significant changes in NDVI are often a result of land cover change, as NDVI is a function of vegetation cover, health and density. NDVI is also an ideal indicator of vegetation biomass. Parameters, such as temperature, precipitation and other climatic variables, are necessary to explain the variances that are exhibited by the NDVI (Chen et al., 2012). Therefore, by studying NDVI, we can learn about not only the land cover changes but also the trends in vegetation degradation and the carbon cycle.

Remotely sensed data provide comprehensive spatial-temporal portraits of long-term vegetation dynamics. Satellite-derived NDVI is a better indicator for studying the actual changes of vegetation on a regional or global scale. In terms of the characteristics of spectral reflectance, green vegetation differs from other land cover types because it strongly absorbs red light with wavelengths of 0.620–0.670 μm and reflects near-infrared light with wavelengths of 0.841–0.876 μm (Huete et al., 2002; Boelman et al., 2003; Tottrup and Rasmussen, 2004). The satellite's spectrometer sensor measures and stores reflectance values for both red and near-infrared bands in two separate channels of images (Huete et al., 2002; Anyamba and Tucker, 2005; Fensholt et al., 2006; Aldakheel, 2011). Many researchers used NDVI as a basic dataset to explore the relationships between NDVI and other factors, such as greenhouse gas concentrations, desertification or climate factors (Suzuki et al., 2001; Guo et al., 2013; Yang et al., 2018). Long-term, coarse-resolution satellite data have been widely used to monitor vegetation productivity for the purposes of mapping land cover changes at regional or global scales. Some scholars have quantified the time series of the Advanced Very High Resolution Radiometer (AVHRR) and the Moderate Resolution Imaging Spectroradiometer (MODIS) vegetation index (NDVI) trends using formal trend tests, including linear regression models (de Beurs and Henebry, 2004; de Jong et al., 2011).

Time series NDVI data have been widely used in detecting the length of the growing period (Vrieling et al., 2013), greening and browning trends (de Jong et al., 2011; Erasmi et al., 2014), vegetation activity change (Jiang et al., 2013) and leaf unfolding dates of forests (Luo et al., 2013). Time series NDVI data have also been used to derive gross primary productivity (GPP) (Wang et al., 2014), vegetation leaf area index (LAI) and fraction of photosynthetically active radiation (FPAR) (Zhu et al., 2013). Additionally, many researchers proposed novel methods to analyze time series NDVI data (Neeti and Eastman, 2011; Pinzon and Tucker, 2014). However, to the best of our knowledge, few research focuses on vegetation trends that related to land use/land cover changes at a global scale; the vegetation trends of different land cover types are also unclear.

The purpose of this study is to quantify the trends of vegetation cover over the past 30+ years, especially for different land cover types. To accomplish this, we first selected 10 samples (4 in arid and semi-arid areas) around the world to explore annual vegetation changes. We investigated the per-pixel NDVI trend using the linear regression model (LM) and Mann-Kendall (MK) trend test based on the NDVI3g.v1 dataset from 1982 to 2015 and compared our results with those of previous studies.

2 Data and Methods

2.1 GIMMS NDVI3g.v1 data

The vegetation index utilizes the differential absorption properties of leaves in different spectral ranges to indirectly measure the amount of green biomass and vegetative health (Tottrup and Rasmussen, 2004; La Puma et

al., 2007). Therefore, the NDVI can be calculated from the spectral specific satellite imagery via the following equation (Equation 1) (Miura et al., 2013):

$$NDVI = \frac{\rho_{nir} - \rho_r}{\rho_{nir} + \rho_r} \quad (1)$$

where ρ_r and ρ_{nir} are the surface reflectance in the red and near-infrared regions of the electromagnetic spectrum, respectively. Arithmetically, NDVI ranges from –1.0 to 1.0, but the actual values at the Earth's surface range from –0.1 to 0.7 (Suzuki et al., 2001).

The NOAA AVHRR satellite series has been operational from 1981 and has provided a long period of data that is unmatched in time scale (Herrmann et al., 2005). The global coverage of NDVI from AVHRR has been regarded as the best dataset available for long-term vegetation trend analyses. The long-term GIMMS NDVI record provides a critical historical perspective on vegetation changes that is necessary for global climate change research and, thus, should be the basis for an intercalibrated, sensor-independent NDVI data record (Brown et al., 2006). This record has been corrected for sensor degradation, inter-sensor differences, solar zenith angle and viewing angle effects due to satellite drift, cloud cover, volcanic aerosols and others not related to vegetation change (Alcaraz-Segura et al., 2010b).

In the present study, the analysis of the vegetation trend was based on the latest version of the NDVI3g.v1 dataset, which was derived from measurements made by AVHRR sensors aboard the National Oceanic and Atmospheric Administration (NOAA) polar-orbiting satellite series (NOAA-7, 9, 11, 14, 16, 17). In fact, NDVI3g.v1 spans the period from July 1981 to December 2015, and the time range used in this paper is from 1982 to 2015, as we will use the annual mean NDVI value. The NDVI3g.v1 data were assembled carefully from different AVHRR sensors accounting for various deleterious effects such as calibration loss, orbital drift, and volcanic eruptions (Wang et al., 2014). The NDVI3g.v1 data used in this study was downloaded from https://ecocast.arc.nasa.gov/data/pub/gimms/3g.v1/, and the database is composed of quasi-15-day composites with a spatial resolution of 1/12 degree. The composite images were obtained using the maximum value composition (MVC) technique (Holben, 1986), which minimizes the influences of atmospheric aerosols and clouds.

2.2 Land cover data

New land cover data, Global Land Cover-SHARE (GLC-SHARE) 2014, were used in this paper (Fig. 1). These data are a new product of the Food and Agriculture Organization of the United Nations (FAO), which combines global land cover data for the first time and provides the most reliable global view of planetary land cover. The spatial resolution of GLC-SHARE 2014 is approximately 1 km, and the data were downloaded from www.glcn.org; more information about the data can be found from this website.

2.3 Mann-Kendall (MK) trend test and the Theil-Sen (TS) estimator

The MK trend test was used in this study, and the test evaluates the degree of similarity between two sets of ranks given to the same object sets. This test uses the number of inversions of pairs of objects that would be required to transform one rank order into another (Kendall, 1938; Hirsch et al., 1982; Valz and Mcleod, 1990; Lanzante, 1996). The data were ranked according to time, and then, each data point was successively treated as a reference data point and was compared to all of the data points that follow in time (Douglas et al., 2000).

The challenge of a successful application of time series analysis is the determination of what constitutes a true change in a remotely sensed variable (e.g., a vegetation index) versus the presence of scene noise (e.g., smoke or cloud contamination) (Neeti et al., 2012). Time series NDVI often do not meet parametric assumptions, such as normality and homoscedasticity. Thus, the temporal trends were calculated as suggested by Alcaraz-Segura et al. (2010a), Alcaraz-Segura et al. (2010b) and Pouliot et al. (2009) using the seasonal MK trend test, a rank-based nonparametric test that is robust against seasonality, non-normality, heteroscedasticity, missing values and both intra- and inter-annual autocorrelation.

The MK trend test determines whether a trend exists for each time scale separately. This test consists of computing the MK statistic (S) (Eqs. 2 and 3) (Dietz and Killeen, 1981; de Beurs and Henebry, 2004; de Jong et al., 2011; Sobrino and Julien, 2011).

$$S = \sum_{k=1}^{n-1} \sum_{j=k+1}^{n} \mathrm{sgn}(x_j - x_k) \quad (2)$$

where

$$\mathrm{sgn}(x_j - x_k) = \begin{cases} -1, & x_j - x_k < 0; \\ 0, & x_j - x_k = 0; \\ 1, & x_j - x_k > 0. \end{cases} \quad (3)$$

and x_j and x_k represent the data points at times j and k ($j > k$), respectively, and n is the number of data points.

It is necessary, however, to compute the probability that is associated with S and the sample size, n, to statistically quantify the significance of the trend. For $n \geq 10$, the statistic S is approximately normally distributed with the mean and variance as follows (Equ. 4) (Douglas *et al.*, 2000; Sobrino and Julien, 2011):

$$Var(s) = \frac{n(n-1)(2n+5) - \sum_{p=1}^{g} t_p(t_p-1)(2t_p+5)}{18} \quad (4)$$

where n is the number of data points, g is the number of tied groups (a tied group is a set of sample data having the same value), and t_p is the number of data points in the pth group. More detailed information can be found in de Jong et al. (2011).

The standardized Z test statistic is computed by Equation 5:

$$Z = \begin{cases} \dfrac{S-1}{\sqrt{Var(S)}}, & S > 0 \\ 0, & S = 0 \\ \dfrac{S+1}{\sqrt{Var(S)}}, & S < 0 \end{cases} \quad (5)$$

The Z statistic fits the standard normal distribution: a positive Z value indicates an upward trend, whereas a negative value indicates a downward trend (Neeti and Eastman, 2011).

To obtain the magnitude of the NDVI trend, a non-parametric method referred to as the Theil-Sen approach (TSA) is used in this paper. This approach provides a more robust slope estimate than that of the least-squares method because outliers or extreme values in the time series have a minimal influence on the result (Sen, 1968). The TSA algorithm is derived by Hirsch et al. (1982) and consists of the median of all of the possible pairwise slopes in the dataset.

The slope of n pairs of data points was estimated using the TS estimator (Sen, 1968; Theil, 1992), which is given by Equation 6:

$$\text{TS slope} = \text{Median}\left(\frac{x_i - x_j}{t_i - t_j}\right) \quad (6)$$

where x_i and x_j are data values at times t_i and t_j ($i > j$), respectively.

The slope that was calculated by the TS estimator is a robust estimate of the magnitude of a trend, and this method has been widely used to identify the slopes of trend lines in hydrological time series (Mohsin and Gough, 2010). The use of the TS slope provides the special benefit of the rejection of inter-annual variability (Neeti and Eastman, 2011).

The MK test requires time series to be serially independent. The presence of a serial correlation in the time series makes trend tests too liberal, i.e., the null hypothesis of no trend is rejected too frequently, especially if there is a positive serial correlation (Some'e et al., 2012). The MK test is applicable only when all of the observations in a time series are serially independent. The trend analysis of each time series requires testing for serial auto-correlation as a first step before applying the MK trend test (Mohsin and Gough, 2010). For this, Neeti and Eastman (2011) suggest that the time series be 'pre-whitened' to eliminate the effect of serial correlation before applying the MK test.

In this paper, we employed the Earth Trends Modeler (ETM) tool, a vertical application within the IDRISI software system (IDRISI Selva Manual, Version 17). The ETM provides a wealth of tools for the analysis of trends and the dynamic characteristics of these phenomena in time series images.

2.4 Data postprocessing

To simplify the calculation, the 15-day GIMMS NDVI3g.v1 was aggregated into monthly values using an MVC approach. Moreover, monthly temporal resolution is used most frequently in climatic and biophysical studies. We also calculated the annual mean NDVI values to analyze the temporal trend of NDVI. In bare regions, the NDVI value is quite low, and its changes are mainly caused by soil reflectance. In this study, we masked the areas with an annual sum NDVI less than 0.15.

Because of haze and cloud affection, missing values also appear in the monthly NDVI data. Spatial interpolation was applied to remove the missing values. Using

this method, the median value of the 3 × 3 pixels that surround the missing value were selected to represent the missing value.

The NDVI time-series contains outliers, seasonal variations and serial auto-correlation. The inverse Fourier transformation, which utilizes the results from a complete forward transformation to reconstruct time-series images, was used to remove or reduce outliers that may be present in a time-series. We used a pre-whitening process (Neeti and Eastman, 2011) to remove the serial autocorrelation of the time-series data.

3 Results

3.1 Temporal trends of NDVI values of 10 samples

To understand the temporal trend of vegetation around the world, we selected 10 samples to reflect the NDVI trend (Fig. 1). Samples were evenly distributed around the world and sufficiently large (approximately 6° × 6°) to contain many land cover types. Our observed areas were mainly focused on arid and sub-arid regions where the NDVI is sensitive to vegetation change. The first sample is in Central America, where the land is mainly covered by cropland and grassland. The second sample is in central Brazil around the Amazon plain, where the land cover types are mainly tree and shrub land. The third sample is located along the boundary of France and Germany, where the land covers are mainly cropland and forest. The fourth sample is along the southern boundary of the Sahara Desert, where the land cover is mainly grassland, cropland and bare soil. The fifth sample is located in the southern Africa, where the land cover is grassland and shrub land. The sixth sample is along the boundary of Kazakhstan and Russia, where the land cover is mainly cropland and sparse vegetation. The seventh sample is in India, where the vegetation is mainly cropland. The eighth sample is along the boundary of Mongolia and China, where the vegetation is mainly grassland, with a large area of sparse vegetation. The ninth sample is in southern China, where cropland and forest are the main vegetation covers. The last sample is in Australia, where the land cover types are mainly sparse vegetation, grassland and cropland. All of the samples were evenly distributed around the world and do not include forest regions.

We calculated the annual mean NDVI value for each sample from 1982 to 2015 and analyzed the linear trend of the NDVI (Fig. 2). Of the 10 samples, we found that the NDVI in the fourth, sixth, eighth and tenth samples show a downward trend. Surprisingly, these 4 samples were all located along the boundary of desert or sandy land, with grassland as the main land cover. These results indicate that the desertification process has become more serious in the past 30+ years and that the outlook for vegetation degradation in arid and semi-arid regions is not optimistic. We also found that, annually, the NDVI fluctuates greatly as vegetation cover was affected by many factors, such as the length of growing season, rainfall or even human activities. Except in the regions around the sandy land, the NDVI showed a

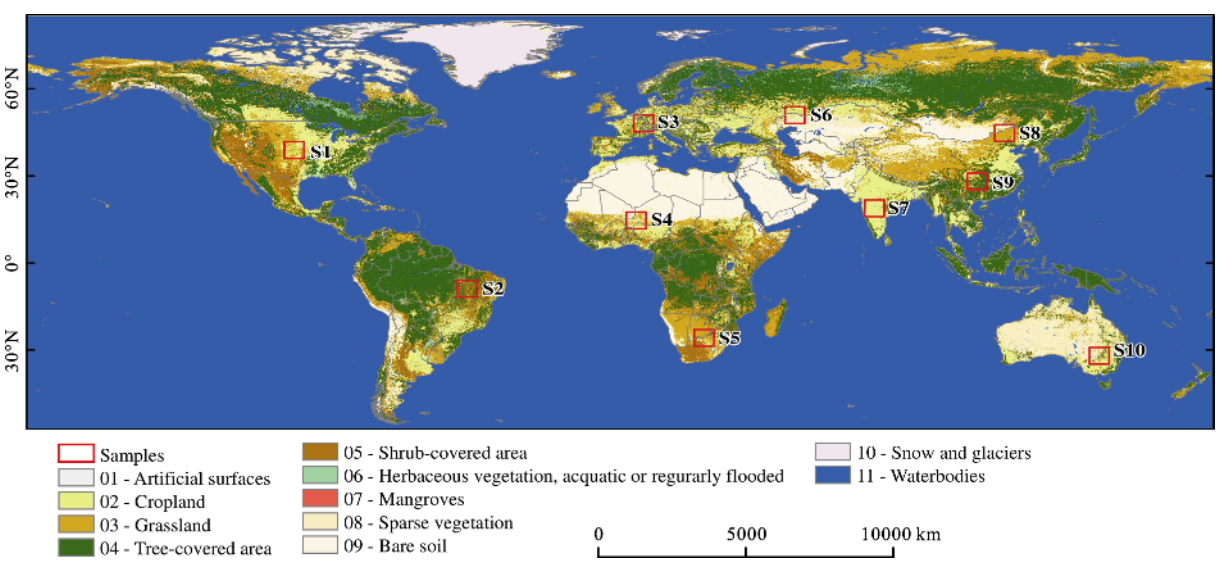

Fig. 1 Land cover types around the world with indicated sample locations. Data were downloaded from the website: http://www.glcn.org/databases/lc_glcshare_en.jsp

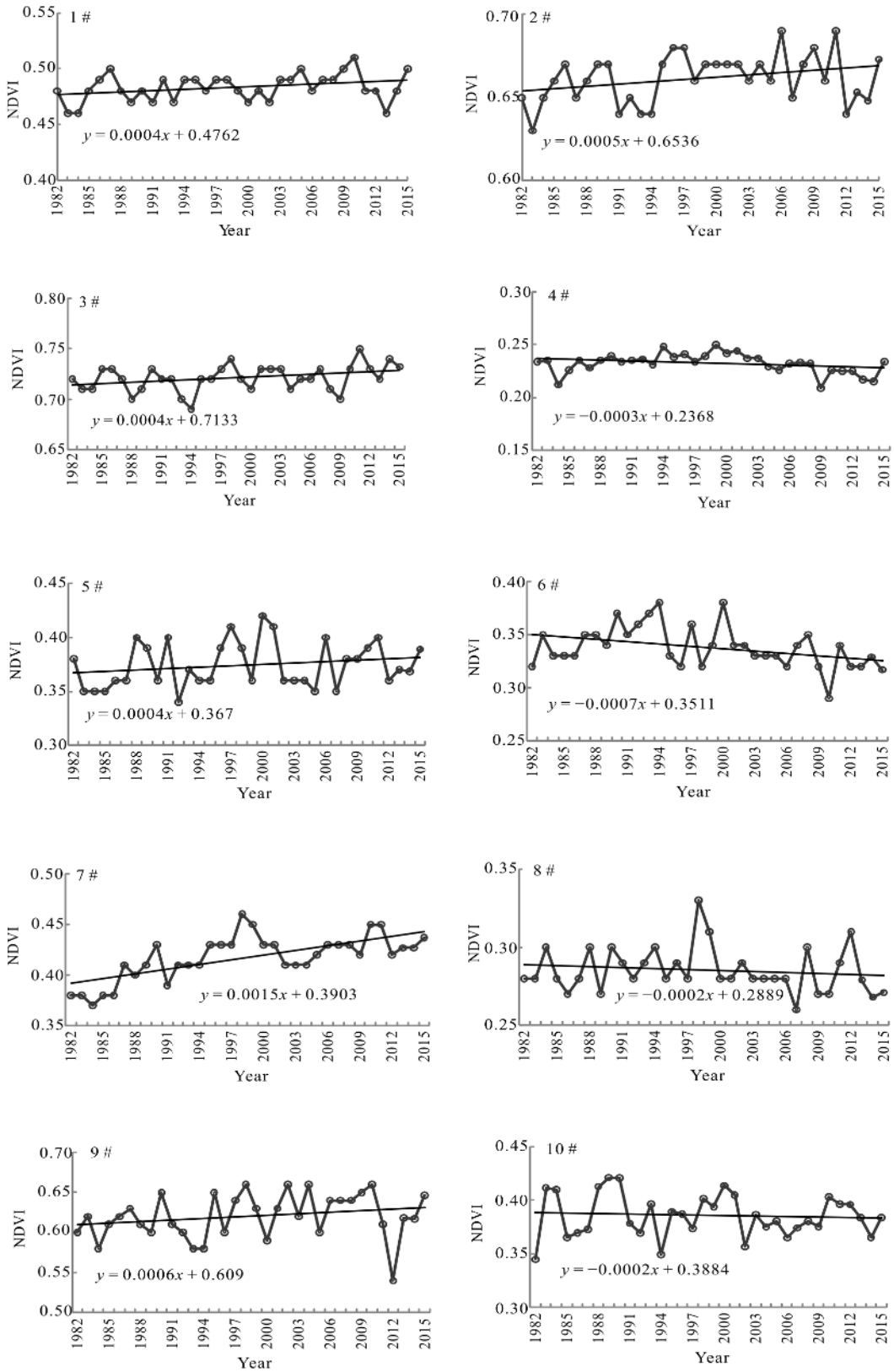

Fig. 2 Annual mean normalized difference vegetation index (NDVI) for each sample

general upward trend, which means that the vegetation cover has partially improved.

3.2 Linear trends of NDVI values

Using a linear regression model, we measured the linear trend of per-pixel NDVI against time (dNDVI/dYear) based on an anomaly dataset (Fig. 3). Fig. 3 shows the NDVI trend against time at the 95% significance level. The blue to red color bar indicates the NDVI trend from 1982 to 2015 decreasing to increasing significantly. We observed that the increasing trend pixel number (83.37%) is greater than the decreasing trend (16.63%), which indicates that the vegetation cover has been improving in most regions over the past 30+ years. Overall, positive trends were apparent in some boreal forest regions of Russia and European countries, North America, central Africa and India. We also saw that vegetation in some parts of central and eastern China, western Europe and central Africa showed a strong positive trend. The negative trends mainly occurred in Canada, southern Latin America, southern Africa and northeastern China.

3.3 Mann-Kendall trend of NDVI

Figs. 4 and 5 showed the MK-Z and TS slope results at the 95% significance level from 1982 to 2015. Here, we masked the desert region regions (NDVI < 0.15) in calculation.

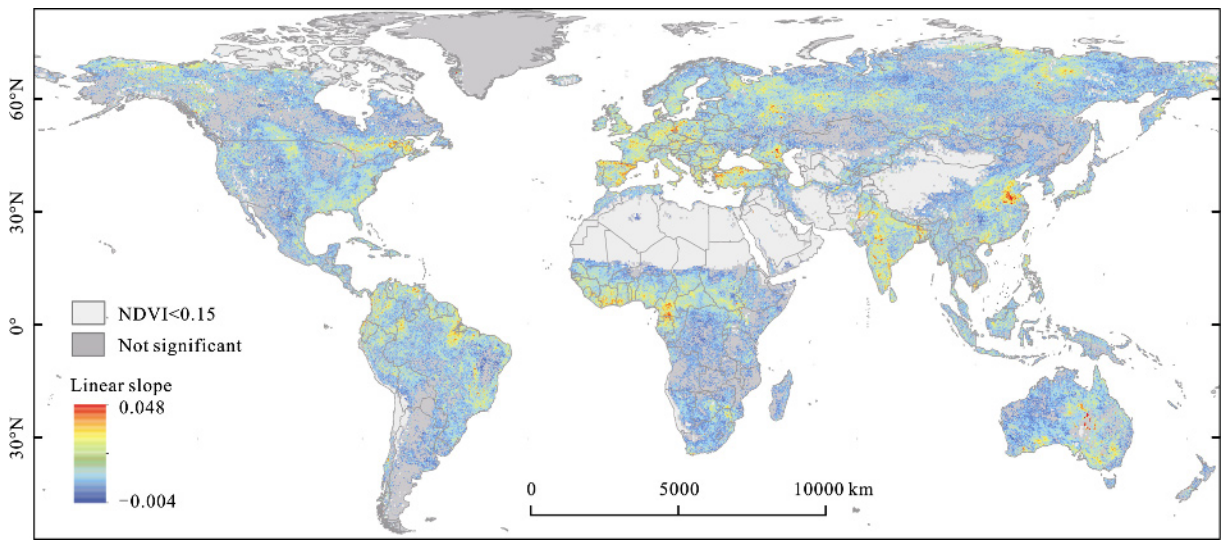

Fig. 3 The annual NDVI trend slope (dNDVI/dYear)

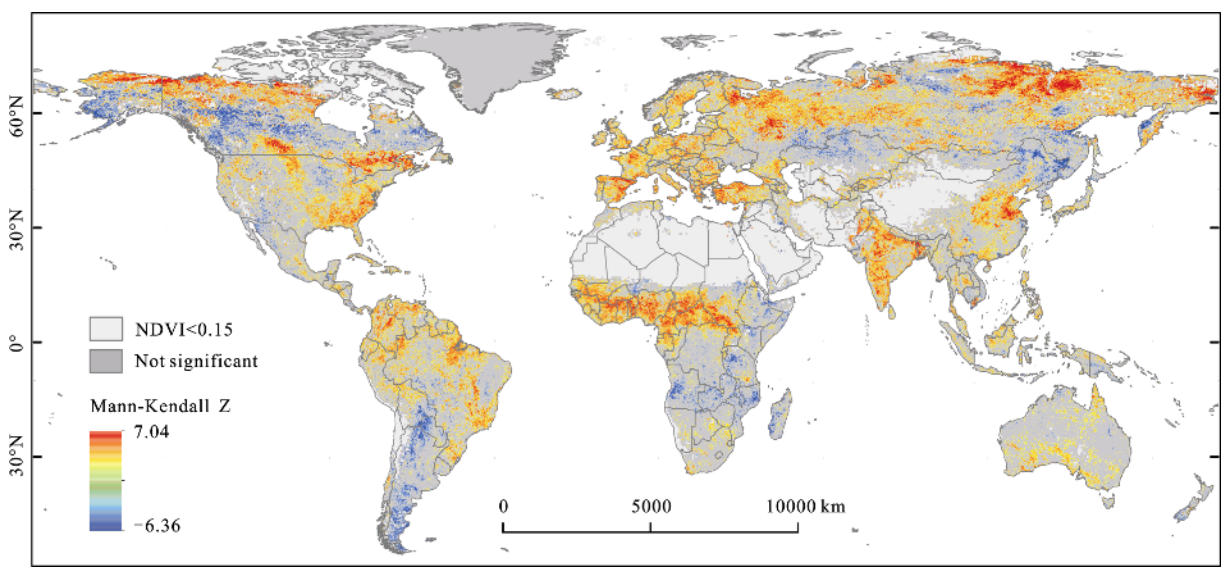

Fig. 4 Per-pixel Mann-Kendall Z value of NDVI from 1982 to 2015

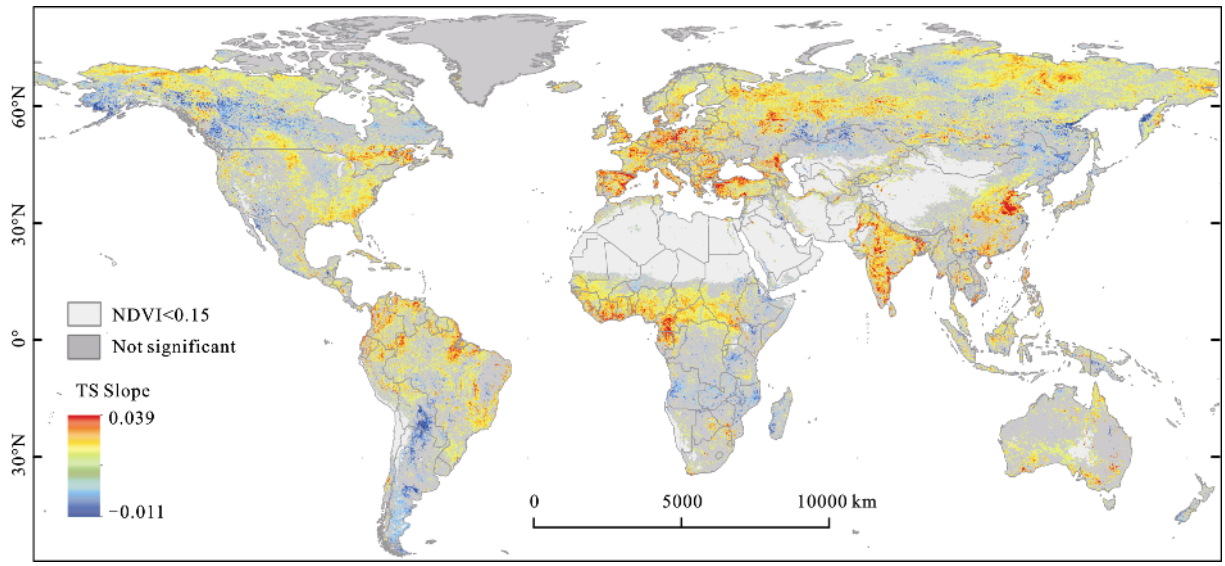

Fig. 5 Per-pixel TS slope value of NDVI from 1982 to 2015

TS slope value trends were similar to those of the MK-Z, with an increasing trend in Europe, Sub-Saharan Africa, India, Northern South America, Eastern America and central China. A decreasing trend occurred in Canada, Southern South America, Southern Africa and Western Asia. In North America, the increasing NDVI trend was focused in northern Alaska, northern and southwestern Canada, and central and western America. The NDVI in some regions of northern and western Latin America exhibited an increasing trend. In central Africa, India, central China and most regions of Europe and Russia, the NDVI showed a sharp increase. The regions with a decreasing trend occurred in central Canada, southern Latin America, southern Africa, northeastern China, central Russia and northern Kazakhstan. With regard to the results of the TS slope and MK-Z results, we observed that the MK-Z captures the existence or absence of positive and negative trends and that the TS slope was able to capture the positive and negative trends as well.

We also found that the trend of the NDVI in the MK-Z and TS slope results were clearer than that of the linear model in most regions. This indicated that the MK trend test was more appropriate than the linear model for the NDVI time series.

4 Discussion

4.1 Assessment of vegetation trends

From the temporal trend of NDVI of the 10 samples, we found that NDVI had a decreasing trend in samples 4, 6, 8 and 10. All of these samples were located in the arid and semi-arid regions and contained parts of desert or sandy land (Fig. 1 and Fig. 2), and sample 6 shows an obvious decreasing trend (linear slope is –0.0007). This result indicates that the vegetation cover around desert or sandy land has a deteriorating trend. Because of the limitation of rainfall, it is difficult for humans to return sandy land to vegetation cover, and it is also difficult to prevent the process of desertification. Our results verified the conclusion of Kaplan et al. (2014), who argued that in Turkmenistan, pastures have shown a high degree of vegetation degradation due to the soil biogenic crust. However, Sternberg et al. (2015) found that from 2000 to 2012, the Gobi area showed a decreasing trend in China and Mongolia, which is contrary to our result. One reason for this difference is because of different time scales, and another reason is that their study only contains Gobi regions. Using NDVI3g data from 1981 to 2011, Dardel et al. (2014) found the same result as we did in the agropastoral Fakara (in a similar location as that of the fourth sample) in that decreasing trends were observed both from the satellite NDVI and field assessments of herbaceous mass. In fact, vegetation cover depends largely on precipitation, especially during the growing seasons (Sternberg et al., 2015). This result also reveals that the desertification process is a serious problem worldwide.

Sample 7 shows larger regression line slopes (0.0015), which indicate that in cropland regions, the NDVI ex-

hibited a growing trend. In sample 9, we see that the NDVI decreased obviously in 2011 and 2012 because of the serious drought in the southeastern China. The samples that containing a mix of shrub land, cropland and grassland regions, the NDVI also showed an increasing trend.

The results of per-pixel slopes from the linear regression model using the annual mean NDVI (Fig. 3) were very close to the linear trend analysis of the yearly cumulative values that calculated the net primary productivity (NPP) from 1981 to 2003 (Bai et al., 2008). Because their study did not show the significance level in the result figure, we could not compare our results with theirs in a more detailed manner. We found some similar results to ours in a study that calculated the NDVI trend using a linear model from 1981 to 2006 (de Jong et al., 2011). In Europe, our results showed not only a positive slope but also a negative trend, but in de Jong et al.'s results, Europe had no negative slope. In Australia, our results are nearly opposite to those of Jong et al.'s which may be because of the different time scales, different datasets and different significance levels.

The MK trend test ranked the data according to time and then obtained the Z value by comparing each data point to all of the following data points (Douglas et al., 2000). We also see that in the MK-Z results, the growing trend of NDVI is obvious compared to that of the linear regression slope results. The TS slope results also have a similar result as that of MK-Z. In the MK-Z and TS slope, the results showed that the decreasing trend of NDVI was less than the linear regression slope results. In addition, we did not observe a decreasing NDVI trend in central Australia. Our MK trend test results were similar to the results of de Jong et al. (2011).

From the results of the linear trend and MK trend test, we concluded that on a global scale, vegetation cover has changed over the past 3 decades. However, a region's initial state with a time series was an inherent problem (de Jong et al., 2011) and affects the NDVI trend. For instance, the drought in the early 1980s in Sahel (Giannini et al., 2008) leaded to a lower vegetation cover during the initial stage of our time scale. The increasing trend of the NDVI may recover from these droughts. Thus, it is difficult to identify the vegetation recovery without climate factors.

4.2 Land cover types in the increasing and decreasing trend of NDVI

We overlaid the *MK-Z* with land cover types. Here, we used the global land cover in 2014 and assumed that there was no land cover change between 2014 and 2015. We found that of the growing trends of NDVI, the land cover in these regions, is mainly forest-covered area (52.63%, sum of the tree-covered and shrub-covered areas), cropland (19.81%) and grassland (18.25%). Of the decreasing trends, forest-covered pixels were dominant 58.65% (sum of 44.32% and 14.33%) (Table 1). The spatial distribution of the NDVI trend in each land cover type can be found in Fig. 6. The increasing trend of the NDVI in tree-covered areas is mainly in Siberia, eastern America and the Amazon. The increasing NDVI in cropland mainly occurred in India, southern Canada and southeastern China. The increasing trend of NDVI in grassland is mainly distributed at a high latitude in northern Russia and northern Canada.

In cropland regions, the NDVI increased in central North America, India and mid-eastern China. This result is primarily because of the increasing area of cropland and the improvement in crop planting technology. In Russia, the NDVI in some tree and shrub regions shows an increasing trend. The main vegetation type in this region is boreal forest, and the increasing trend of the

Table 1 Ratio of the increasing and decreasing trends for each land cover type (%)

	02	03	04	05	06	08	09	Sum
Increasing*	19.81	18.25	44.73	7.90	2.29	5.06	1.97	100
Decreasing*	13.00	14.73	44.32	14.33	2.63	6.91	4.09	100
Increasing	16.51	15.21	37.30	6.58	1.91	4.22	1.64	83.37
Decreasing	2.16	2.45	7.37	2.38	0.44	1.15	0.68	16.63

Notes: Here, we calculated the main changed land cover types. Increasing* (decreasing*) means an increasing pixel rate of each land cover to the increased (decreased) sum. Increasing (decreasing) means the increasing pixel rate of each land cover to the changed (both increased and decreased) sum. The numbers 02, 03, 04, 05, 06, 08 and 09 indicate cropland, grassland, tree-covered area, shrub-covered area, herbaceous vegetation or aquatic or regularly flooded, sparse vegetation and bare soil, respectively, as shown in Fig. 1. Here, we did not show the other land cover types whose changes were not clear

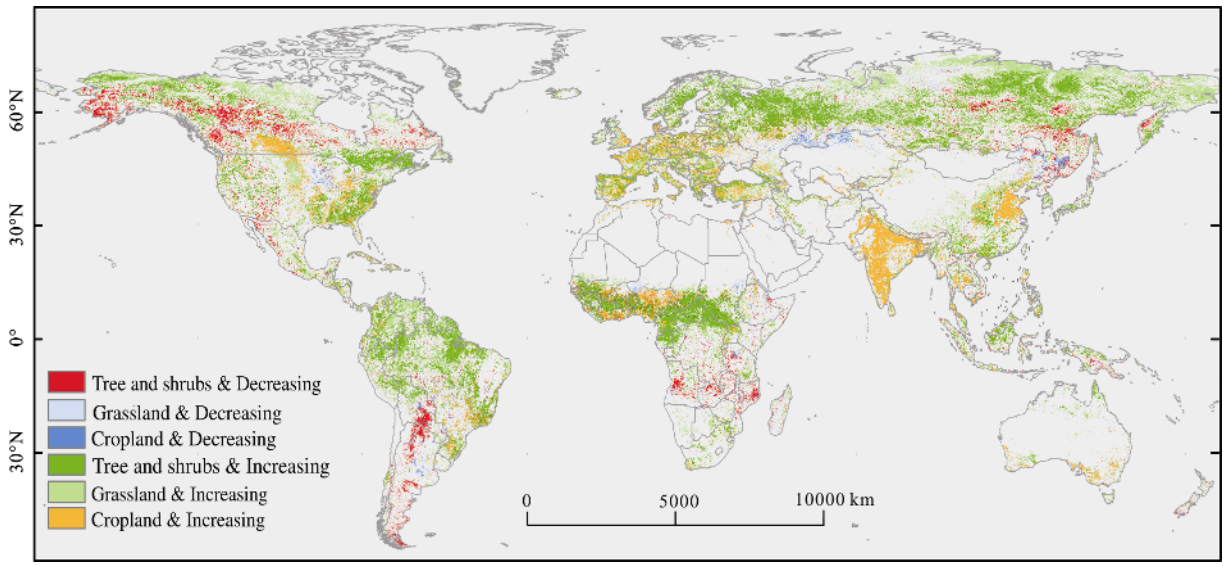

Fig. 6 Land cover changes overlaid with the increasing and decreasing NDVI

NDVI is primarily because of the growth and re-growth of forest and may also because of the vegetation succession after a disturbance. The decreasing trend of the NDVI in this region may be because of fire disturbances and human logging.

Fig. 6 also shows that in Sanjiang Plain of northeastern China, the NDVI decreased obviously. Sanjiang Plain used to be the largest wetland in China, but now it has been one of the major paddy rice production areas in China. After more than 40 year's exploitation, its wetland area has decreased sharply (Na et al., 2007). Vegetation cover from marsh wetland, which has a higher biomass than that of paddy rice, is the main reason for the NDVI decrease.

4.3 Accuracy of the vegetation trends

In this paper, we used the monthly NDVI to calculate the global trend of vegetation cover. Because of the interference of snow cover, atmospheric aerosols, and clouds, the monthly NDVI values often deviate from their nominal values, and the NDVI trend may also be affected. Some other disturbances, such as forest fire, flood, drought and human activities, also affected the trend of the NDVI. But we did not consider those factors in this study.

The NDVI can reach saturation in dense vegetation canopies, such as in forests (Huete et al., 1997) and cropland (Gu et al., 2013) in growing seasons, which may lead to a biased trend in high (dense) biomass regions. Fig. 6 shows that regions with increasing NDVI are mainly focused in tree and shrub land and in India, central and east China and central North America and some increased NDVI also occurred in cropland. Because of a higher vegetation density, in forest and cropland, the NDVI may reach saturation and affect the NDVI trend. As we observed, because of the higher reflectance of bare land and lower density of vegetation cover, the NDVI values were lower than the true value in arid and semi-arid regions. The NDVI trend in these regions may be affected by soil reflectance which were did not consider in this paper.

5 Summary and Conclusions

The time-series GIMMS NDVI dataset has been widely used to analyze the global changes that are related to vegetation because it is the longest-duration vegetation-cover dataset available. In this study, we used GIMMS NDVI3g.v1 data from 1982 to 2015 to evaluate the global vegetation trends. Some useful conclusions were obtained:

(1) We selected 10 samples around the world representing different land cover types in different regions and found that in the samples from the arid and semi-arid regions, the NDVI showed a decreasing trend and that in other regions, the NDVI increased. These results indicate that the vegetation cover deteriorated in some arid regions.

(2) The linear regression model and MK trend test were used to analyze the spatial distribution of NDVI

changes around the world. We found similar results as those of previous researchers in some regions, but because of different significance levels, different time scales and different data processes, we also found some different results in some regions.

(3) By overlaying the NDVI trend and land cover types, we found that increasing NDVI values mainly occurred in forest-covered areas, cropland and grassland. A decreasing NDVI trend also primarily occurred in tree-covered regions.

References

Alcaraz-Segura D, Chuvieco E, Epstein H E et al., 2010a. Debating the greening vs. browning of the North American boreal forest: differences between satellite datasets. *Global Change Biology*, 16(2): 760–770. doi: 10.1111/j.1365-2486.2009.01956.x

Alcaraz-Segura D, Liras E, Tabik S et al., 2010b. Evaluating the consistency of the 1982–1999 NDVI Trends in the Iberian peninsula across four time-series derived from the AVHRR sensor: LTDR, GIMMS, FASIR, and PAL-II. *Sensors*, 10(2): 1291–1314. doi: 10.3390/s100201291

Aldakheel Y, 2011. Assessing NDVI spatial pattern as related to irrigation and soil salinity management in al-hassa oasis, Saudi Arabia. *Journal of the Indian Society of Remote Sensing*, 39(2): 171–180. doi: 10.1007/s12524-010-0057-z

Anyamba A, Tucker C J, 2005. Analysis of sahelian vegetation dynamics using NOAA-AVHRR NDVI data from 1981–2003. *Journal of Arid Environments*, 63(3): 596–614. doi: 10.1016/j.jaridenv.2005.03.007

Bai Z G, Dent D L, Olsson L et al., 2008. Proxy global assessment of land degradation. *Soil Use and Management*, 24(3): 223–234. doi: 10.1111/j.1475-2743.2008.00169.x

Barrow C J, 2009. Desertification. In: Kitchin R, Thrift N (eds). *International Encyclopedia of Human Geography*. Oxford: Elsevier, 96–101.

Boelman N T, Stieglitz M, Rueth H M et al., 2003. Response of NDVI, biomass, and ecosystem gas exchange to long-term warming and fertilization in wet sedge tundra. *Oecologia*, 135(3): 414–421. doi: 10.1007/S00442-003-1198-3

Brown M E, Pinzon J E, Didan K et al., 2006. Evaluation of the consistency of long-term NDVI time series derived from AVHRR, SPOT-vegetation, SeaWiFS, MODIS, and Landsat ETM+ sensors. *IEEE Transactions on Geoscience and Remote Sensing*, 44(7): 1787–1793. doi: 10.1109/TGRS.2005.860205

Chen Z J, Li J B, Fang K Y et al., 2012. Seasonal dynamics of vegetation over the past 100 years inferred from tree rings and climate in Hulunbei'er steppe, northern China. *Journal of Arid Environments*, 83: 86–93. doi: 10.1016/j.jaridenv.2012.03.013

Dardel C, Kergoat L, Hiernaux P et al., 2014. Re-greening Sahel: 30 years of remote sensing data and field observations (Mali, Niger). *Remote Sensing of Environment*, 140: 350–364. doi: 10.1016/j.rse.2013.09.011

de Beurs K M, Henebry G M, 2004. Trend analysis of the Pathfinder AVHRR Land (PAL) NDVI data for the deserts of central Asia. *IEEE Geoscience and Remote Sensing Letters*, 1(4): 282–286. doi: 10.1109/LGRS.2004.834805

de Jong R, de Bruin S, de Wit A et al., 2011. Analysis of monotonic greening and browning trends from global NDVI time-series. *Remote Sensing of Environment*, 115(2): 692–702. doi: 10.1016/j.rse.2010.10.011

Dietz E J, Killeen T J, 1981. A nonparametric multivariate test for monotone trend with pharmaceutical applications. *Journal of the American Statistical Association*, 76(373): 169–174. doi: 10.1080/01621459.1981.10477624

Douglas E M, Vogel R M, Kroll C N, 2000. Trends in floods and low flows in the United States: impact of spatial correlation. *Journal of Hydrology*, 240(1–2): 90–105. doi: 10.1016/S0022-1694(00)00336-X

El Hassan I M, 2004. Desertification monitoring using remote sensing technology. In: *Proceeding of the International Conference on Water Resources and Arid Environment*. Saudi Arabia: King Saud University.

Erasmi S, Schucknecht A, Barbosa M et al., 2014. Vegetation greenness in northeastern brazil and its relation to ENSO warm events. *Remote Sensing*, 6(4): 3041–3058. doi: 10.3390/rs6043041

Fensholt R, Sandholt I, Stisen S et al., 2006. Analysing NDVI for the African continent using the geostationary meteosat second generation SEVIRI sensor. *Remote Sensing of Environment*, 101(2): 212–229. doi: 10.1016/j.rse.2005.11.013

Giannini A, Biasutti M, Verstraete M M, 2008. A climate model-based review of drought in the Sahel: Desertification, the re-greening and climate change. *Global Planet Change*, 64: 119–128. doi: 10.1016/j.gloplacha.2008.05.004

Gu Y X, Wylie B K, Howard D M et al., 2013. NDVI saturation adjustment: a new approach for improving cropland performance estimates in the Greater Platte River Basin, USA. *Ecological Indicators*, 30: 1–6. doi: 10.1016/j.ecolind.2013.01.041

Guo M, Wang X F, Li J et al., 2013. Spatial distribution of greenhouse gas concentrations in arid and semi-arid regions: a case study in East Asia. *Journal of Arid Environments*, 91: 119–128. doi: 10.1016/j.jaridenv.2013.01.001

Herrmann S M, Anyamba A, Tucker C J, 2005. Recent trends in vegetation dynamics in the African Sahel and their relationship to climate. *Global Environmental Change*, 15(4): 394–404. doi: 10.1016/j.gloenvcha.2005.08.004

Hirsch R M, Slack J R, Smith R A, 1982. Techniques of trend analysis for monthly water quality data. *Water Resources Research*, 18(1): 107–121. doi: 10.1029/WR018i001p00107

Holben B N, 1986. Characteristics of maximum-value composite images from temporal AVHRR data. *International Journal of Remote Sensing*, 7(11): 1417–1434. doi: 10.1080/01431168608948945

Huete A, Didan K, Miura T et al., 2002. Overview of the radiometric and biophysical performance of the MODIS vegetation indices. *Remote Sensing of Environment*, 83(1–2): 195–213.

doi: 10.1016/S0034-4257(02)00096-2

Huete A R, Liu H Q, van Leeuwen W J D, 1997. The use of vegetation indices in forested regions: issues of linearity and saturation. *Proceedings of the IGARSS'97. 1997 IEEE International Geoscience and Remote Sensing Symposium Proceedings*. *Remote Sensing - A Scientific Vision for Sustainable Development*. Singapore, Singapore: IEEE, 1964: 1966–1968. doi: 10.1109/IGARSS.1997.609169

Jiang N, Zhu W Q, Zheng Z T et al., 2013. A comparative analysis between GIMSS NDVIg and NDVI3g for monitoring vegetation activity change in the northern hemisphere during 1982–2008. *Remote Sensing*, 5(8): 4031–4044. doi: 10.3390/rs5084031

Kaplan S, Blumberg D G, Mamedov E et al., 2014. Land-use change and land degradation in Turkmenistan in the post-Soviet era. *Journal of Arid Environments*, 103: 96–106. doi: 10.1016/j.jaridenv.2013.12.004

Kendall M G, 1938. A new measure of rank correlation. *Biometrika*, 30(1–2): 81–93. doi: 10.1093/biomet/30.1-2.81

La Puma I P, Philippi T E, Oberbauer S F, 2007. Relating NDVI to ecosystem CO_2 exchange patterns in response to season length and soil warming manipulations in arctic Alaska. *Remote Sensing of Environment*, 109(2): 225–236. doi: 10.1016/j.rse.2007.01.001

Lanzante J R, 1996. Resistant, robust and non-parametric techniques for the analysis of climate data: theory and examples, including applications to historical radiosonde station data. *International Journal of Climatology*, 16(11): 1197–1226. doi: 10.1002/(SICI)1097-0088(199611)16:11<1197::AID-JOC89>3.0.CO;2-L

Luo X Z, Chen X Q, Xu L et al., 2013. Assessing performance of NDVI and NDVI3g in monitoring leafUnfolding dates of the deciduous broadleaf forest in Northern China. *Remote Sensing*, 5(2): 845–861. doi: 10.3390/rs5020845

Miura T, Turner J P, Huete A R, 2013. Spectral compatibility of the NDVI Across VIIRS, MODIS, and AVHRR: an analysis of atmospheric effects using EO-1 Hyperion. *IEEE Transactions on Geoscience and Remote Sensing*, 51(3): 1349–1359. doi: 10.1109/TGRS.2012.2224118

Mohsin T, Gough W A, 2010. Trend analysis of long-term temperature time series in the Greater Toronto Area (GTA). *Theoretical and Applied Climatology*, 101(3–4): 311–327. doi: 10.1007/s00704-009-0214-x

Na Xiaodong, Zhang Shuqing, Li Xiaofeng et al., 2007. Application of MODIS NDVI time series to extracting wetland vegetation information in the Sanjiang plain. *Wetland Science*, 5(3): 227–236. (in Chinese)

Neeti N, Eastman J R, 2011. A contextual Mann-Kendall approach for the assessment of trend significance in image time series. *Transactions in Gis*, 15(5): 599–611. doi: 10.1111/j.1467-9671.2011.01280.x

Neeti N, Rogan J, Christman Z, et al., 2012. Mapping seasonal trends in vegetation using AVHRR-NDVI time series in the Yucatán Peninsula, Mexico. *Remote Sensing Letters*, 3(5): 433–442. doi: 10.1080/01431161.2011.616238

Pinzon J E, Tucker C J, 2014. A non-stationary 1981–2012 AVHRR $NDVI_{3g}$ time series. *Remote Sensing*, 6(8): 6929–6960. doi: 10.3390/rs6086929

Pouliot D, Latifovic R, Olthof I, 2009. Trends in vegetation NDVI from 1 km AVHRR data over Canada for the period 1985–2006. *International Journal of Remote Sensing*, 30(1): 149–168. doi: 10.1080/01431160802302090

Prince S D, Beckerreshef I, Rishmawi K, 2009. Detection and mapping of long-term land degradation using local net production scaling: application to Zimbabwe. *Remote Sensing of Environment*, 113(5): 1046–1057. doi: 10.1016/j.rse.2009.01.016

Sen P K, 1968. Estimates of the regression coefficient based on Kendall's Tau. *Journal of the American Statistical Association*, 63(324): 1379–1389.

Sobrino J A, Julien Y, 2011. Global trends in NDVI-derived parameters obtained from GIMMS data. *International Journal of Remote Sensing*, 32(15): 4267–4279. doi: 10.1080/01431161.2010.486414

Some'e B S, Ezani A, Tabari H, 2012. Spatiotemporal trends and change point of precipitation in Iran. *Atmospheric Research*, 113: 1–12. doi: 10.1016/j.atmosres.2012.04.016

Stellmes M, Udelhoven T, Röder A et al., 2010. Dryland observation at local and regional scale: Comparison of Landsat TM/ETM+ and NOAA AVHRR time series. *Remote Sensing of Environment*, 114(10): 2111–2125. doi: 10.1016/j.rse.2010.04.016

Sternberg T, Rueff H, Middleton N, 2015. Contraction of the Gobi desert, 2000–2012. *Remote Sensing*, 7(2): 1346–1358. doi: 10.3390/rs70201346

Suzuki R, Nomaki T, Yasunari T, 2001. Spatial distribution and its seasonality of satellite-derived vegetation index (NDVI) and climate in Siberia. *International Journal of Climatology*, 21(11): 1321–1335. doi: 10.1002/joc.653

Theil H, 1992. A rank-invariant method of linear and polynomial regression analysis. In: Raj B, Koerts J (eds). *Henri Theil's Contributions to Economics and Econometrics*. Houten, the Netherlands: Springer, 345–381.

Tottrup C, Rasmussen M S, 2004. Mapping long-term changes in savannah crop productivity in Senegal through trend analysis of time series of remote sensing data. *Agriculture, Ecosystems & Environment*, 103(3): 545–560. doi: 10.1016/j.agee.2003.11.009

Tucker C, 1979. Red and photographic infrared linear combinations for monitoring vegetation. *Remote Sensing of Environment*, 8(2): 127–150. doi: 10.1016/0034-4257(79)90013-0

Valz P D, McLeod A I, 1990. A simplified derivation of the variance of Kendall's rank correlation coefficient. *The American Statistician*, 44(1): 39–40. doi: 10.2307/2684956

Vrieling A, de Leeuw J, Said M Y, 2013. Length of growing period over Africa: variability and trends from 30 years of NDVI time series. *Remote Sensing*, 5(2): 982–1000. doi: 10.3390/rs5020982

Wang J B, Dong J W, Liu J Y, et al., 2014. Comparison of gross primary productivity derived from GIMMS NDVI3g, GIMMS, and MODIS in Southeast Asia. *Remote Sensing*, 6(3): 2108–2133. doi: 10.3390/rs6032108

Yang J, Sun J, Ge Q S et al., 2017. Assessing the impacts of urbanization-associated green space on urban land surface temperature: a case study of Dalian, China. *Urban Forestry & Urban Greening*. 22:1–10. doi: 10.1016/j.ufug.2017.01.002.

Yang J, Guan Y Y, Xia J H et al., 2018. Spatiotemporal variations characteristics of green space ecosystem service value at urban fringes: a case study on Ganjingzi District in Dalian, China. *Science of the Total Environment*. 639: 1453–1461. doi: 10.1016/j.scitotenv.2018.05.253.

Zeng F W, Collatz G J, Pinzon J E et al., 2013. Evaluating and quantifying the climate-driven interannual variability in global inventory modeling and mapping studies (GIMMS) normalized difference vegetation index (NDVI3g) at global scales. *Remote Sensing*, 5(8): 3918–3950. doi: 10.3390/rs5083918

Zhu Z C, Bi J, Pan Y Z et al., 2013. Global data sets of vegetation leaf area index (LAI)3g and fraction of photosynthetically active radiation (FPAR)3g derived from global inventory modeling and mapping studies (GIMMS) normalized difference vegetation index (NDVI3g) for the period 1981 to 2011. *Remote Sensing*, 5(2): 927–948. doi: 10.3390/rs5020927